



# Biaxial Extension of Cruciform Specimens: Embedding Equilibrium Into Design and Constitutive Characterization

G. Vitucci<sup>1</sup>

Received: 8 August 2023 / Accepted: 29 February 2024  
© The Author(s) 2024

## Abstract

**Background** Main desired features of biaxial tests are: uniformity of stresses and strains; high strain levels in gauge areas; reliable constitutive parameters identification. Despite cruciform specimen suitability to modern tensile devices, standard testing techniques are still debated because of difficulties in matching these demands.

**Objective** This work aims at providing rational performance objectives and efficient cruciform specimens shapes in view of constitutive characterization.

**Methods** Objective performance is evaluated along particular lines lying on principal directions in equibiaxial tensile tests. A rich specimen profile geometry is purposely optimized via finite elements analysis by varying cost function and material compressibility. Experimental tests, monitored via digital image correlation, are carried out for validation.

**Results** New shapes are designed and tested in a biaxial tensile apparatus and show to perform better than existing ones. Elastic parameter identification is efficiently performed by only exploiting full field strain measurements along statically significant lines.

**Conclusions** Small gauge areas and small fillet radii cruciform specimens approach the ideal deformation behaviour. For the constitutive parameters identification in planar tensile experiments, it suffices to monitor strains along the gauge lines.

**Keywords** Biaxial testing · Shape optimization · Cruciform specimen · Uniform strain · Gauge area · Load transmission · FEM based design

## Introduction

An ideal biaxial tensile experiment would reproduce an homogeneous specimen deformation, so that predictions of constitutive models could be promptly tested on a range of deformation classes minimizing the need of *ad hoc* numerical tools and inverse analysis. Nevertheless available experimental data are scarce. For instance, in the recent work [1], neural networks have been developed for rubberlike constitutive model discovery. The most recent biaxial dataset used as database in that paper is [2], which dates back to 1962.

Traditionally, the difficulty in obtaining reliable data have been due to lack of equipment in common research facilities. Nowadays, despite a broader availability of biaxial tensile machines, the experimental mechanics literature is still

flourishing about the design of specimens which satisfy certain kinematic and static constraints upon loading since no universally accepted shapes for biaxial test exist [3]. Already in the work [4], conceptual criteria were introduced to delineate the expected behavior of an ideal cruciform specimen for extracting precise constitutive information from biaxial tests. They can be summarized as obtaining, in a large test zone: a homogeneous deformation; a high strain level. The homogeneity is required for easily comparing predictions to experiments; the high strain level allows exploring large material deformations without incurring into failure outside the test zone. Both goals are hard to achieve, because gauge areas boundary conditions are affected by the substructures transferring loads from the device grips.

A range of topological solutions have been proposed, based on which of the two aforementioned objectives an improvement is sought for (e.g. see reviews in [4–6]). Clearly, boundary conditions affect strain distributions within the gauge area [7]. Although linear guides, by letting the clamping zone expand without shear, have been

✉ G. Vitucci  
gennaro.vitucci@poliba.it

<sup>1</sup> DICATECh, Polytechnic University of Bari, Via Re David 200, Bari 70125, Italy

utilized in the past (e.g. [2, 8]), this system requires multiple connections, personnel interaction during tests and can not provide real time data. Clamping, on the other hand, is the standard and most widely adopted gripping method, but it induces shear which affects biaxiality in the tested zone [9]. As a remedy, long or slotted arms have been tested. In this way, the specimen arms result more compliant and the gauge strain level decreases [10]. As an alternative, simple or double hinges and sutures or hooks have been engineered, but such discretization of load application heavily localizes strains with possible failure around holes [7]. On the contrary, stiffer load transfer, obtained by reducing thickness in the test area [11–13], stiffening or enlarging the arms end up worsening biaxiality [14].

With this work, we aim at contributing toward an experimental approach which: can be both easily reproduced with common mechanical laboratory tools; tested by means of widely adopted tensile machines and grips; requires minimal specimen machining for common materials usually supplied as sheets; can return useful information to be promptly compared with theoretical predictions. To this end, we deal with constant thickness, compact thin cruciform specimens, i.e. without holes or slots, whose arms are clamped in the device grips. As design variable, only the specimen profile shape is considered, by adopting a five degrees of freedom smooth single curve, in order to avoid profile discontinuity at the source of strain concentration [15].

High biaxiality has been the goal of, among others, the shape optimizations conducted in [14, 16, 17]. Mixed specimen quality criteria, also including high strain levels, have been adopted by [10, 18–21]. Both these performance objectives are examined also in the present work. The main novelty with respect to existing literature consists in the simultaneous adoption of: a weighted multi-objective cost function which enables investigating the extent by which either of the two objectives influences the optimized shape and performance; a systematic optimization procedure which is based on measurable, material independent errors, expressed in terms of strain invariants; the computation of errors along a line, rather than in significative points or across whole surfaces. This line-evaluated error enables the establishment of a direct relationship between immeasurable stresses and forces through equilibrium. Error integration along lines has already been adopted by [10], but the considered lines did not statically isolate the specimen portion and the load cells from the remaining structure. As shown hereinafter, our choice, independent of the reference frame, significantly simplifies constitutive parameters identification, without the need for computationally costly numerical simulations.

As a case study, the proposed criteria are applied, in the framework of infinitesimal strain theory, for designing cruciform samples and identifying their elastic constants. Our optimization based design is carried out by means of the finite element method (FEM) and it prospects a set of optimal

shapes depending on objectives weights and material parameters. These novel shapes are cut from a polymeric material and tested in equibiaxial experiments together with specimens borrowed from literature. The gauge area strain field is reconstructed by digital image correlation (DIC), as this is a very versatile and cost effective strain monitoring technique [22, 23]. The performance of different shapes is analyzed in terms of: efficiency according to the newly proposed error measures; effectiveness in parameter identification [24].

## Theory

Hereafter, the ideal deformation state of a cruciform specimen subject to a biaxial test is described, in the particular case of equibiaxiality. Keeping this goal in mind, the discrepancy between actual kinematics and performance objectives can be quantified so that a set of FEM optimized shapes can be designed. Achieving this involves modulating a highly flexible smooth profile geometry and modelling its mechanical response in linear theory. Finally, parameter identification procedures are established.

## Performance Objectives

Attaining perfect equibiaxiality in large areas of clamped specimens proves challenging. An intuitive explanation is that an equibiaxial deformation is a homothetic transformation. Clamping, though, prevents transversal expansion of cruciform sample arms and this induces shear. In order to quantify a specimen suitability for equibiaxial tensile tests, measures of the discrepancy between an ideal and the experimental case need to be introduced. In an equibiaxial tensile test on an ideal specimen, the experimenter would impose a macroscopic stretch  $\bar{\epsilon}$  and obtain an equibiaxial deformation in a known specimen area. It is convenient to deal with principal strains, since they are independent on reference frame. Thus, in every point  $\mathbf{x}$ , the infinitesimal strain tensor, expressed in the planar principal frame, would thus take the matrix form:

$$\begin{bmatrix} e_1(\mathbf{x}) & 0 \\ 0 & e_2(\mathbf{x}) \end{bmatrix} = \begin{bmatrix} \bar{\epsilon} & 0 \\ 0 & \bar{\epsilon} \end{bmatrix} \forall \mathbf{x} \in \text{tested zone}, \quad (1)$$

where the subscript 1 and 2 refer to the first and second strain principal directions and  $e_i$  are the principal strains, with  $e_1 > e_2$ . As a result, once defined the maximum planar shearing strain  $\Delta(\mathbf{x})$  and the average principal strain  $\Sigma(\mathbf{x})$ , one would aim at:

$$\Delta(\mathbf{x}) := \frac{e_1(\mathbf{x}) - e_2(\mathbf{x})}{2} = 0. \quad (2a)$$

$$\Sigma(\mathbf{x}) := \frac{e_1(\mathbf{x}) + e_2(\mathbf{x})}{2} = \bar{\varepsilon}, \quad (2b)$$

Accordingly, we introduce two integral errors based on these quantities. Namely, the first one measures the loss of equibiaxiality and the second one quantifies the loss of strain as follows:

$$\eta_{\Delta} = \frac{1}{\bar{\varepsilon}} \sqrt{\frac{\int_{OC} \Delta^2(s) ds}{OC}}, \quad (3a)$$

$$\eta_{\Sigma} = \frac{1}{\bar{\varepsilon}} \sqrt{\frac{\int_{OC} (\Sigma(s) - \bar{\varepsilon})^2 ds}{OC}}. \quad (3b)$$

It is noteworthy that these two errors can be interpreted as standard deviations from the expected (ideal) performance and are computed on the whole gauge line OC, (see Fig. 1). Whereas in previous works similar norms have already been used (e.g. [13, 24]), here it is proposed the selection of a geometric entity, for the integrals in equation (3), which allows for statically isolating a part of the structure. In two dimensional settings, such an entity should be a line, since surfaces or points do not allow to directly extract resulting forces. In other words, the external force  $F$  measured at the clamps level can be directly related to the average stress state  $\sigma$  along the whole gauge line. This is important in view of constitutive investigations, given that, while deformations can be estimated by full field measurements, stresses can only be inferred in an integral sense from the machine load cell. Furthermore, if the strain field is known along a line, it would be computationally inexpensive to assign such a state to elements on that line and to retrieve the total exerted force instead of simulating the whole structure behavior for deducing material parameters. Other scholars have preferred obtaining uniform stress rather than strain state (e.g. [14]), but this: complicates the mathematical

treatment, since constitutive equations are usually expressed in the form of stress as a function of strain; requires a device controlled in force, which is unusual.

Generally, the pursuit of low  $\eta_{\Delta}$  and  $\eta_{\Sigma}$  may lead to conflicting solutions. For this reason, in view of an optimized design, we finally group them into one indicator

$$\eta = (1 - \alpha)\eta_{\Delta} + \alpha\eta_{\Sigma}, \quad (4)$$

where the parameter  $\alpha \in [0, 1]$  is used to build a weighted sum multi-objective function. Here, a value of  $\alpha = 0$  or 1 shifts all the objective towards a low  $\eta_{\Delta}$  or low  $\eta_{\Sigma}$ , respectively.

## Specimen Shape

For the sake of manufacturing simplicity, we restrict our geometry to a simply connected surface, i.e. without holes, and constant thickness, as most materials are produced in sheets. Furthermore, the introduction of slots causes the arms to elongate more than the gauge area, thus lowering  $\eta_{\Sigma}$ . Cross-shaped specimens are widely used in biaxial tests because of their suitability to modern tensile machines. These, indeed, have four controllable arms where to clamp the material. As the specimen extremities are usually constrained to rectilinear segments, the only aspect requiring design is its profile.

In theory, various choices could be considered for the parametrization of the sample profile. It has however been noted that the profile should be as continuous as possible in order to avoid stress concentrations from where cracks could nucleate (e.g. see [25] and literature therein). A family of functions which guarantees smoothness and flexibility is splines and in particular we opt for third degree B-splines, since B-splines are: optimal in a mathematical sense from the point of view of support and smoothness; ubiquitous in computer-aided design which is the main tool for technical drawing (e.g. [26]).

Five parameters are selected for drawing the specimen profile, as illustrated in Fig. 1, and these are the degrees of freedom of the B-spline control points A,B,T,C, where A and C have triple multiplicity. Specifically,  $y_A$  represents the clamping length,  $x_C$  identifies the coordinate of point C along the  $\pi/4$  bisector,  $x_T$  governs the curvature in C, and the coordinates of point B ( $x_B, y_B$ ) determine the slope and curvature in A, introducing the possibility of a point of inflection along AC. Note that line CT is orthogonal to OC to preserve smoothness across the diagonal symmetry. Therefore, only one of  $x_T$  or  $y_T$  can be chosen independently. This way, the profile shape is defined by the vector

$$\Gamma = [y_A, x_C, x_T, x_B, y_B], \quad (5)$$

with the constraint that the control points polygonal CTBA stays inscribed in the isosceles right rectangle OLO' of unitary catheters.

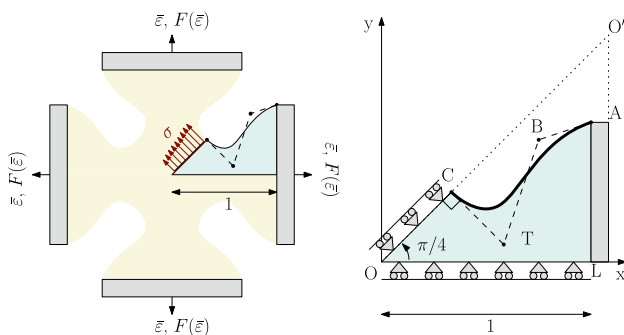


**Fig. 1** Geometry definition of the cruciform specimen and mechanical problem. One eighth of the specimen and its symmetry axes are represented under equibiaxial loading. Its profile is determined by cubic B-splines whose control points are A, B, T, C. The profile shape parameters are the coordinates  $y_A$ ,  $x_B$ ,  $y_B$ ,  $x_T$  and  $x_C$

## Mechanical Model

The thickness of the investigated flat cruciform specimen is small relative to the gauge area dimension. Given that the specimen is stretched by the machine in its plane, we assume the validity of the classical plane stress hypothesis. The applied boundary conditions are of Dirichlet type on the clamps, meaning that clamping imposes a constant displacement in the machine arms axial direction and zero displacement in the arms transverse direction. This is representative of a typical experimental setting, where the arms are clamped inside rigidly translating grips. Displacements are imposed at the grips level, in an attempt to cause an equibiaxial state in the inner specimen area. The problem symmetries can be exploited from a computational standpoint since they allow for simulating only one-eighth of the area by introducing sliding constraints along the lines OC and OL (see Fig. 1).

In this work, the material is considered isotropic and linearly elastic. Therefore, its constitutive behavior can be fully described by two material parameters only: the Young's modulus and the Poisson's ratio  $\nu$ .

## Optimized Specimen Design

Finally, in the quest for the most suitable specimen profile shapes, we utilize the shape degrees of freedom described above and formulate the following constrained optimization problem:

$$\begin{aligned} \min_{\Gamma} \quad & \eta(\Gamma, \alpha, \boldsymbol{\mu}) = (1 - \alpha)\eta_{\Delta}(\Gamma, \boldsymbol{\mu}) + \alpha\eta_{\Sigma}(\Gamma, \boldsymbol{\mu}), \\ \text{with} \quad & \mathbf{0} < \Gamma < \mathbf{1}, \\ & x_C < x_T < 2x_C, \\ & x_T, y_B < x_B, \end{aligned} \quad (6)$$

where  $\mathbf{0}$  and  $\mathbf{1}$  are the null and all-ones vectors, respectively, of the same size as  $\Gamma$ . These linear inequality constraints are introduced to inscribe the specimen eighth in the triangle  $OLO'$  as motivated in the previous paragraph. The symbol  $\boldsymbol{\mu}$  collects material properties which are introduced in order to investigate the effect of constitutive features onto the specimen shape design. In this way, the solution of equation (6) is able to return the optimal specimen geometry as a function of the objective weights and material properties, i.e.  $\Gamma = \Gamma(\alpha, \boldsymbol{\mu})$ .

Considering deformation variables only, under imposed Dirichlet conditions, the Young's modulus does not play any role, as it only scales stresses and forces. Conversely, Poisson's ratio clearly affects strain inhomogeneity in biaxial tests, as it represents interactions between orthogonal fibres. Only its influence is consequently explored, so that in equation (6)  $\boldsymbol{\mu} = \nu$ .

In terms of software, both geometry and domain decomposition (meshing) were accomplished using the open source package Gmsh [27]. The mesh was created using the standard Delaunay triangulation algorithm with curvature based mesh refinement and comprised about two thousands triangular linear finite elements.

The elasticity equations were solved by using the open source FEM software Elmer [28] through its wrapper Pyelmer [29]. The plane stress settings allowed overcoming the volumetric locking associated with high Poisson's ratios. The geometry and FEM software was interfaced via Python. In this way, we were able to conduct the multi-objective constrained optimization above. In particular, we adopted the trust region algorithm `trust-constr`, available via Scipy [30].

During the constrained multi-objective optimization process, the errors  $\eta_{\Delta}$  and  $\eta_{\Sigma}$  were computed for each simulation in order to reach the optimum. To this purpose, a Python script was developed which can extract the FEM data along the line OC and compute the strain invariants and the integrals needed for evaluating the objective function equation (6).

## Constitutive Parameters Identification

The central task associated to extension tests is the identification of material properties. Ideal tests would set a straightforward correspondence between load cell data and stress versus strain curves. However ideal biaxial tests are challenging to perform. Here a novel procedure is proposed which exploits equilibrium considerations and full field deformation measurements. These measurements are nowadays commonly obtained by analysing the test footage, for example as described later in the experimental section. This way, the extension test output are the load cell forces  $F(\bar{\epsilon})$  and typically the displacement field  $\mathbf{u}(\mathbf{x}, \bar{\epsilon})$  for every timestep or macrostrain  $\bar{\epsilon}$ . Given the displacement field, the planar strain tensor  $\mathbf{E}(\mathbf{x}, \bar{\epsilon})$  is reconstructed together with the displacement gradient. A particular strain tensor, e.g. infinitesimal, Cauchy-Green, Green-Lagrange, etc., is selected based on the investigated constitutive model. It is furthermore commonplace that constitutive models are expressed in terms of strain tensor invariants, which in the planar case are just two,  $I_1$  and  $I_2$ . In this study, these two latter fields are interpolated along the gauge line OC via the local coordinate  $s$  running along OC, i.e. one obtains  $I_1(s, \bar{\epsilon})$  and  $I_2(s, \bar{\epsilon})$ .

Commonly, the constitutive model predicts normal stresses  $\sigma_n$  as a function of strain invariants [1, 31, 32], whereas the selection of OC along a symmetry axis, in the case of isotropy, guarantees zero tangential stress  $\tau_n(s) = 0$ . The stress vs strain relation is mediated by a set of material constants  $\boldsymbol{\mu}$  as

$$\sigma_n = \sigma_n(I_1(s, \bar{\epsilon}), I_2(s, \bar{\epsilon}), \boldsymbol{\mu}). \quad (7)$$

Finally, by looking at Fig. 1, the equilibrium can be enforced as

$$\frac{F(\bar{\epsilon})}{2} = \frac{1}{\sqrt{2}} \int_{OC} \sigma_n(s, \bar{\epsilon}, \boldsymbol{\mu}) ds \quad (8)$$

at every macrostrain level  $\bar{\epsilon}$ . The latter is a—in general non-linear—equation in the unknowns  $\boldsymbol{\mu}$ . The proposed material characterization procedure is summarized in Fig. 2.

As a remark, equation (8) requires isotropy, which leads to symmetries and zero tangential strains along OC, but not linearity in the constitutive model and can therefore be applied to finite strain theory. Moreover, notice that the equilibrium equation (8) would not necessitate full-field displacement measurements if an ideal equibiaxial deformation state were achieved in the neighbourhood of any point  $\mathbf{x}$  lying along OC, i.e. for homotetic transformations. In this ideal case,  $\bar{\epsilon}$  would just be imposed at the clamps level.

As a first application, in this study mechanical parameters identification is limited to isotropy and small strains, so that only linear theory is used. This naturally leads to use the infinitesimal strain tensor as the deformation measure. The two considered invariants are  $\Delta$  and  $\Sigma$  as defined in equation (2). Moreover, linearity allows to account for

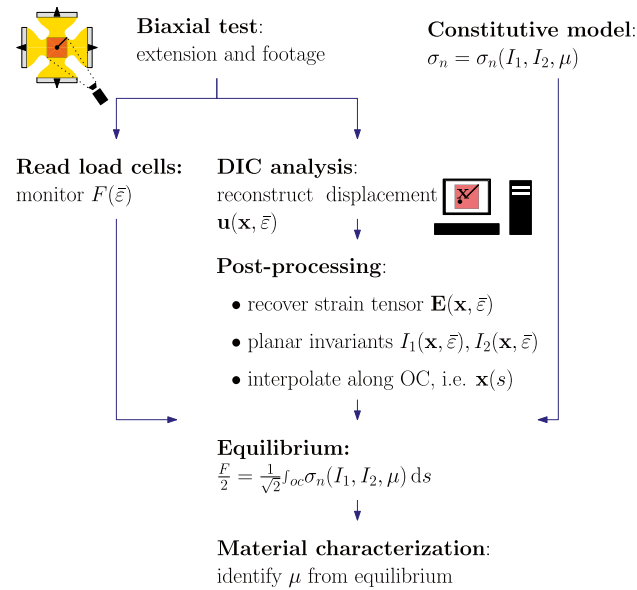


**Fig. 2** Equilibrium motivated material characterization via DIC assisted biaxial extension test. The key concept is the equilibrium based comparison between load cell forces  $F$  and normal stresses  $\sigma_n$  predicted by the constitutive model in order to identify the material properties  $\boldsymbol{\mu}$ . This operation is made possible by the DIC analysis and its post-processing, which return the two planar strain tensor invariants  $I_i$  along the gauge line OC

only one macrostrain  $\bar{\epsilon}$ , which is thus dropped from the following formulae. In plane stress isotropic elasticity, the maximum and minimum principal stresses therefore result

$$\sigma_{\max/\min} = \frac{E}{1-\nu^2} (\Sigma(1+\nu) \pm \Delta(1-\nu)). \quad (9)$$

From Fig. 1, the specimen eighth equilibrium to horizontal translation equation (8) can easily be written as

$$\begin{aligned} \frac{F}{2} &= h \sin \frac{\pi}{4} \int_0^{x_C} \cos \frac{\pi}{4} \sigma_{\max}(\Sigma, \Delta, s) ds \\ &= h \sin \frac{\pi}{4} \langle \sigma_{\max} \rangle \frac{x_C}{\cos \frac{\pi}{4}} \\ &= hx_C \langle \sigma_{\max} \rangle, \end{aligned} \quad (10)$$

where  $\sigma_{\max}$  is given in equation (9),  $F$  is the force read by the load cell and  $h$  is the sample thickness. The symbol  $\langle \cdot \rangle$  denotes averaging along the gauge line.

When utilizing only extension machine data, the strain distribution information is limited, except for the average stretch  $\bar{\epsilon}$  of the horizontal and vertical central lines in Fig. 1. Therefore, assuming  $\Sigma = \bar{\epsilon}$  and  $\Delta = 0$  along the gauge line and substituting these values into equations (9)–(10), yields the Young modulus estimate

$$\text{machine} \rightarrow \tilde{E} = \frac{1-\nu F}{2hx_C \bar{\epsilon}}. \quad (11)$$

For a slightly more informed estimate, an extensometer can be placed in the specimen middle, since, as confirmed by DIC analysis, in that point (of coordinate  $s = 0$ ) the tangential strain is null. Instead of placing such a physical device, the specimen center point DIC data were used. For doing so,  $\Sigma(0)$  can directly substitute  $\bar{\epsilon}$  into equation (11) to obtain

$$\text{DIC}_{(0,0)} \rightarrow \tilde{E} = \frac{1-\nu F}{2hx_C \Sigma(0)}. \quad (12)$$

Applying the superposition principle to equation (10), due to small strains, the average principal stress can be computed by summation of the contributions of average areal strain and average tangential strain from equation (9). This leads to

$$\text{DIC}_{\Delta,\Sigma} \rightarrow \tilde{E} = \frac{1-\nu^2}{2hx_C} \frac{F}{\langle \Sigma \rangle (1+\nu) + \langle \Delta \rangle (1-\nu)}. \quad (13)$$

## Experimental Procedure

To assess the effectiveness of the present approach in generating suitable shapes and serving as a practical tool for elastic properties identification, an experimental investigation on rubberlike specimens was conducted. The specimens were hand cut from

a 1.4mm thick EPDM sheet with a clamp-to-clamp distance of 110mm. The biaxial tensile machine, produced by Damo Srl, was controlled in displacement on four independent motors and the forces, measured by the four load cells, were monitored. A square area of side  $2x_c$  in the specimen center was painted in white dots for creating a suitable speckle pattern in view of DIC analysis. The extension velocity was set as to provide a low machine strain rate of  $4 \cdot 10^{-4} \text{s}^{-1}$  for dissipating viscosity.

The tests were filmed with a Basler acA1920-155um camera with a Sony IMX174 CMOS sensor at 2.3 MP resolution on  $1920 \times 1200$  pixels. The camera was positioned so that the samples center of mass appeared approximately in the frame middle. The vertical distance between lens and object plane was fixed at about 220mm.

The obtained images were DIC analyzed by means of Ncorr, a common DIC package for Matlab [33]. For the sake of simplicity in phase of data analysis, square regions of interest (ROI) were drawn over the gauge area.

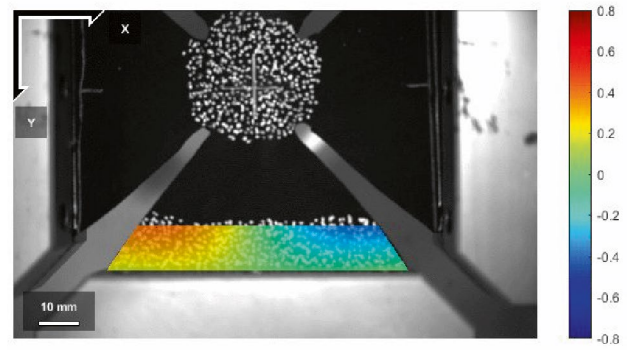
The DIC output, which included the infinitesimal strain tensor components for every pixel, allowed for retrieving the strain invariants, trace and determinant, and from there  $\Sigma$  and  $\Delta$ . These were linearly interpolated along the gauge line and used to determine the experimental performance losses  $\eta_\Delta$  and  $\eta_\Sigma$  as defined in equation (3).

The specimens arms were gripped between two anti-slip aluminium surfaces (see Fig. 3(a)). These were blocked by three bolts for a depth of 15mm each behind the unsupported area. In order to check the validity of the boundary conditions imposed in the FEM simulations, a monotonic equibiaxial extension test was realized up to a 15% macrostrain. The boundary conditions discrepancy is quantified by means of two slippage errors, measuring slippage parallel and perpendicular to the pulling direction (direction  $y$  and  $x$  in Fig. 3(a)). These errors, calculated along the bottom line of the trapezoidal region of interest in figure, are defined as follows:

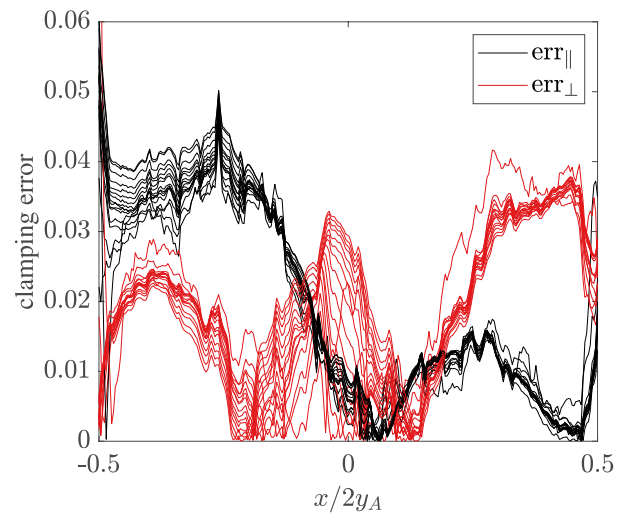
$$\begin{aligned} \text{err}_\parallel(x) &= \left\| \frac{u_\parallel(x)}{\bar{u}} \right\|, \\ \text{err}_\perp(x) &= \left\| \frac{u_\perp(x)}{\bar{u}} - 1 \right\|. \end{aligned} \quad (14)$$

Here,  $\bar{u}$  is the clamp displacement and  $x$  runs along the clamped boundary line. In Fig. 3(b), it is shown that both errors stay below 5% during the whole biaxial extension test. This validates the no-slip condition assumed in the mechanical model.

A material mechanical characterization independent on equibiaxial testing was carried out for validation purposes. A rectangular strip of  $10 \times 110 \text{mm}^2$  was slowly elongated up to a 1% strain. The DIC analysis was carried out on a square area of  $10 \times 10 \text{mm}^2$  in the specimen middle. The Young modulus was estimated as 7.61MPa from the force-elongation data at the machine level. The same modulus was identified by computing the average principal strain along the sample symmetry



(a) DIC



(b) error

**Fig. 3** Slippage at clamps. Equibiaxial extension up to 15% macrostrain. **a** DIC analysis, map of the horizontal displacements near the clamps at 10% macrostrain. **b** Clamping error. Normalized slippage in the direction parallel and perpendicular to the pull vs normalized clamping line coordinate. The clamping line lies at the bottom of trapezoidal region of interest in figure, are defined as follows:

line transversal to loading. When measured in this way, the modulus resulted 7.88MPa, i.e. the gap between the two methods was only about 3.5%. This served as validation for the DIC analysis. Moreover, this difference is justifiable from a mechanical point of view. Clamping does not indeed produce an exactly uniform uniaxial strain on rectangular strips and therefore reading only load cells data might lead to small errors for a planar aspect ratio of 10.

Subsequently, the EPDM Poisson's ratio was inferred by DIC assisted full field strain measurement of the same uniaxial test. The average ratio of the strain parallel and perpendicular to the loading axis was measured along the symmetry line perpendicular to loading and it returned a Poisson's ratio of  $\nu = 0.39$ .

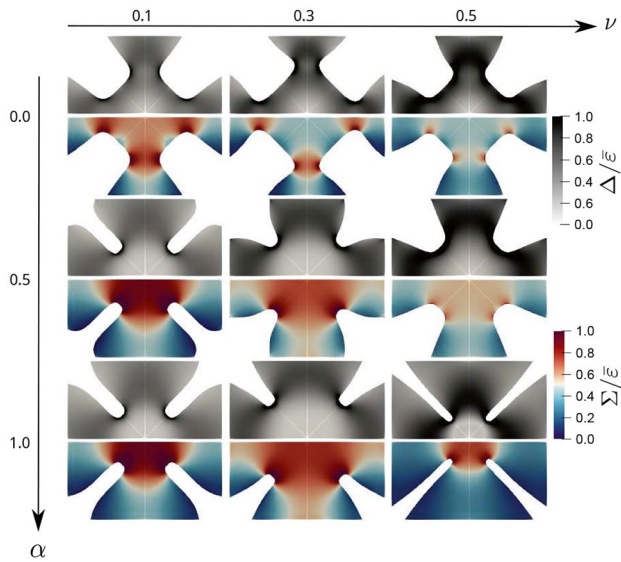


**Fig. 4** Effect of objective function and Poisson's ratio on the FEM optimized design and strain field. The maximum tangential strain  $\Delta$  and the average principal strain  $\Sigma$  are shown in the specimens upper- and lower-halves respectively with the same color mapping. The Poisson's ratio takes the value of 0.1, 0.3 and 0.5 (left to right), the objective function weight  $\alpha$  is 0, 0.5 and 1 (top to bottom)

## Results

The FEM based optimization equation (6) was carried out by letting vary both the Poisson's ratio  $\nu \in \{0.1, 0.3, 0.5\}$  and the objective function weight  $\alpha \in \{0, 0.5, 1\}$  in order to explore the influence of these parameters onto the obtained shapes. The  $3 \times 3$  resulting profiles are shown in Fig. 4, where the computed maximum tangential strain  $\Delta$  and half aerial strain  $\Sigma$  are also depicted.

It is clear that a high  $\nu$  worsens both equibiaxiality degree and transmission of strain from the clamps toward the gauge area. The simulations show indeed that the biaxiality and strain losses can greatly grow when  $\nu$  increases from 0.1 to 0.5 (see Table 1). Next, optimal shapes depend on material behavior via  $\nu$ . Nevertheless, by keeping fixed  $\alpha$ , the optimal shapes do not change dramatically, as it can be noticed by

visually inspecting the rows of Fig. 4. The design variable which shows the highest correlation with  $\nu$  is the coordinate  $x_B$ , whose linear regression returns a negative slope of 0.242 (slope p-value 0.062). A significant correlation is found also for the distance of B from the origin, with a negative slope of 0.403 (slope p-value 0.032). In words, simulations prospect that high Poisson's ratio specimens should be designed with small curvatures in the tract near the clamps.

The multi-objective weight  $\alpha$ , as expected, also affects optimal strain transmission and biaxiality. High  $\alpha$  appear to concentrate  $\Sigma$  in the specimen center. From a geometric point of view, a high  $\alpha$  requires small fillet radii and large clamping length  $y_A$ . This can be interpreted as follows: if the arms are large in comparison with the gauge area, they result stiffer, thus allowing for a higher deformation level in the specimen middle, similarly to reinforced arms specimens. For low  $\alpha$  instead, the optimization algorithm picks large fillet radii with the effect of shifting the areas of high tangential strain far from the gauge line and towards the decentralized fillets. Quantitatively, for same  $\nu$ ,  $\eta_\Delta$  is far less adjustable than  $\eta_\Sigma$ .

The three optimized shapes shown in the third column of Fig. 4, named A00, A05, A10 hereafter, have been selected for experimental testing. The reason for this particular choice lies in an attempt to propose design solutions which can be adopted regardless of *a priori* knowledge of constitutive material behavior. Since, from FEM analysis, incompressible materials result the worst performing, the choice of shapes obtained with  $\nu = 0.5$  appear the most conservative. Furthermore, for comparison with previously proposed designs, two more specimens, whose shapes were borrowed from [6], were cut from the same EPDM sheet. The five specimens were subjected to equibiaxial extension, in displacement control, and their gauge area full field deformation was inferred by postprocessing the filmed images in the square gauge area defined by the vertex C of Fig. 1. The DIC analysis allowed returning the strains in the Cartesian frame (see Fig. 5). From these measurements, the planar strain invariants were reconstructed and our invariant based strain measures  $\Delta$  and  $\Sigma$  were obtained.

**Table 1** Optimization results. Profile shape dependency obtained via multi-objective optimization for combinations of Poisson's ratio  $\nu$  and objective weight  $\alpha$

$\nu$	$\alpha$	$\eta_\Delta$	$\eta_\Sigma$	$y_A$	$x_C$	$x_T$	$x_B$	$y_B$
0.1	0.0	0.31	0.43	0.49	0.33	0.54	0.75	0.32
0.1	0.5	0.34	0.07	0.64	0.33	0.41	0.81	0.71
0.1	1.0	0.35	0.05	0.70	0.29	0.38	0.75	0.64
0.3	0.0	0.35	0.60	0.51	0.36	0.64	0.80	0.34
0.3	0.5	0.45	0.23	0.48	0.41	0.47	0.73	0.50
0.3	1.0	0.45	0.18	0.72	0.45	0.51	0.67	0.55
0.5	0.0	0.51	0.59	0.44	0.33	0.52	0.69	0.32
0.5	0.5	0.57	0.44	0.50	0.38	0.49	0.73	0.39
0.5	1.0	0.71	0.22	0.83	0.23	0.27	0.60	0.54

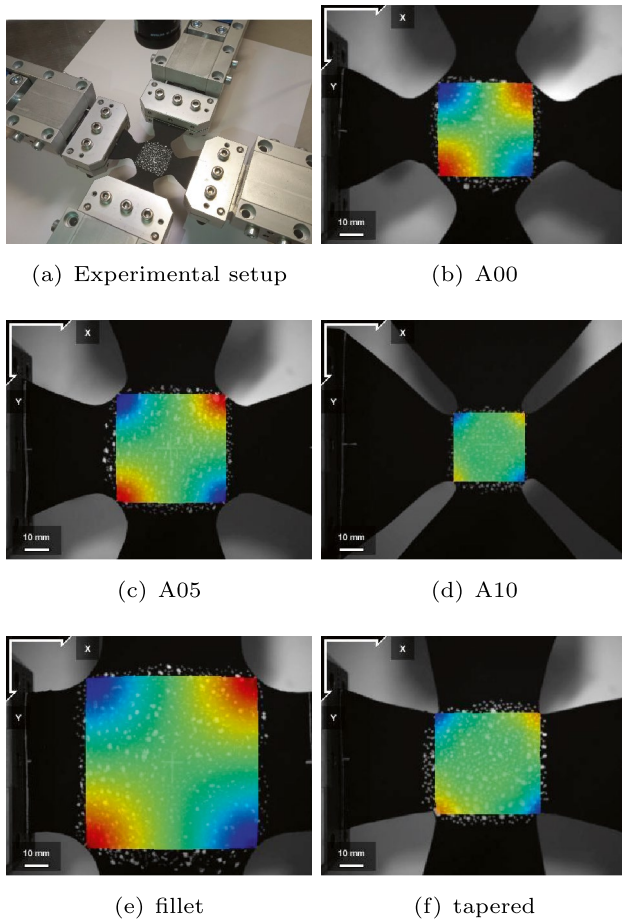


**Fig. 5** Equibiaxial tensile tests and full field measurements. Polymeric cruciform specimens were gripped in the biaxial tensile machine and subjected to equibiaxial tensile tests. The full-field strain measurements were obtained by means of DIC. In **b** to **f** the shearing strain  $\epsilon_{xy}$  in the Cartesian frame, as directly obtained by the DIC software, is shown. Blue and red zones, concentrated around corners, map high absolute values of  $\epsilon_{xy}$

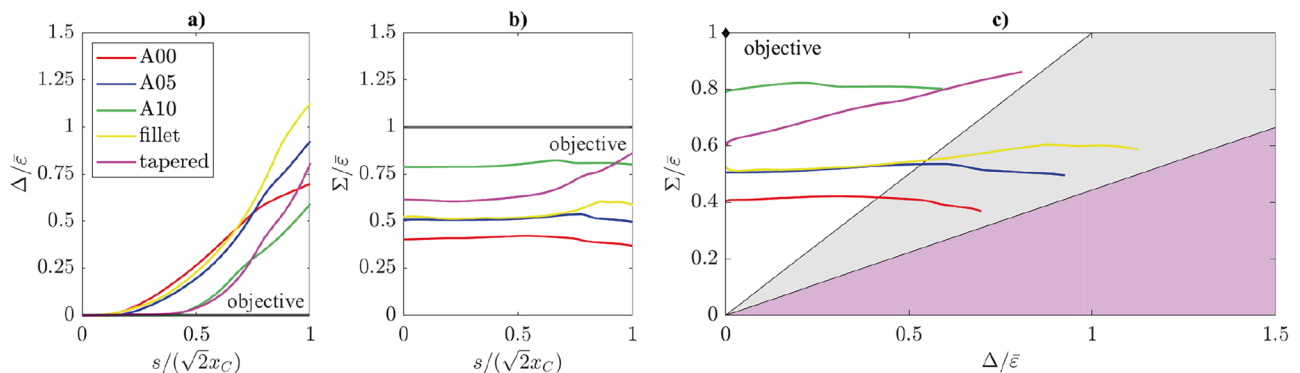


**Fig. 6** Experimental strains from DIC analysis. The gauge line planar strains  $\Delta$  and  $\Sigma$  were reconstructed from DIC analyses for the five tested specimens. All strains are normalized by the imposed machine strain  $\bar{\epsilon} = 1\%$ . **a** and **b**  $\Delta$  and  $\Sigma$ . **c**  $\Sigma$  versus  $\Delta$ . The grey and magenta areas mean respectively contraction and compression in at least one direction

These ROI full field data for  $\Delta$  and  $\Sigma$  were interpolated along the gauge line and plotted in Fig. 6. In Fig. 6(a) the five  $\Delta(s)$  curves are compared. The lowest biaxiality loss were achieved by our A10 and the tapered specimens with an  $\eta_{\Delta}$  of 0.23 and 0.29, respectively (see Table 2). Both curves departed from the ideal zero  $\Delta$  at a distance of about 50% the gauge line length. Surprisingly, the other three specimens, i.e. A00, A05 and the fillet profiles, performed markedly worse, reaching a maximum  $\Delta$  close to  $\bar{\epsilon}$  and departing from zero in the vicinity of the gauge area center of mass, even though large fillet radii resulted favorable to lower tangential strains from FEM simulations.

Also regarding strain transmission, our A10 and the tapered specimens resulted the most efficient, with a loss  $\eta_{\Sigma}$  of 0.20 and 0.34. The latter sample was though less constant in  $\Sigma(s)$ , with a tendency to grow from the gauge center outwards. The other three profiles attained a higher strain loss, but all remained approximately constant along the gauge line. This result agrees well with the simulations, as it can be noticed by comparing the A00, A05 and A10  $\eta_{\Sigma}$  of Table 2 with the  $\eta_{\Sigma}$  corresponding to  $\nu = 0.5$  in Table 1.

In an attempt to elucidate the source of high  $\eta_{\Delta}$  for the three specimens with large fillet radii,  $\Delta$  and  $\Sigma$  have been plotted against each other in Fig. 6(c). There, it can be observed that our A10 and the tapered specimens were the closest to the global objective of minimizing both strain and biaxiality loss. In our tests, the principal directions of maximum and minimum normal stress are the gauge line and its perpendicular, respectively. Consequently, by adopting the minus sign in equation (9), it results that all three large fillet radii specimens reached very low positive stresses towards the fillet and a large portion of the gauge line contracted, whereas it would be expected to expand if the gauge area were uniformly stretched (grey area  $\Delta < \Sigma$  in Fig. 6(c)).



**Table 2** Experimental biaxiality and strain transmission errors

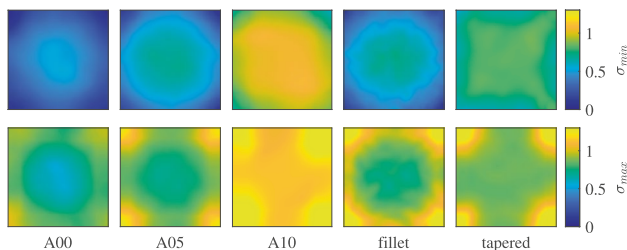
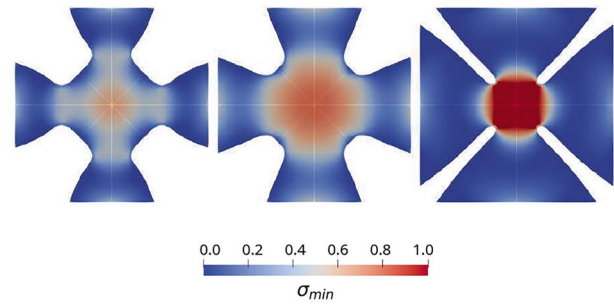
	A00	A05	A10	fillet	tapered
$\eta_{\Delta}$	0.39	0.42	0.23	0.50	0.29
$\eta_{\Sigma}$	0.59	0.49	0.20	0.46	0.34

Principal stresses are mapped across the ROIs of all samples in Fig. 7. Very low minimum principal stresses, loosely speaking the radial ones, were retrieved for the A00, A05 and fillet shapes, thus confirming what has been noted along the gauge line. The highest minimum gauge stress arose in A10, followed by the tapered specimen. This latter showed peculiar X-shaped stress isolines, with minimum stress loss along its ROI edges rather than in corners. The maximum principal stresses, roughly the hoop ones, attained their peak around the corners and were not qualitatively different across samples. The A10 profile produced the highest mean.

The deformation out of the gauge area was not monitored by DIC analysis. Therefore, for what concerns the specimen arms, simulations must be relied upon. The FEM minimum principal stresses are depicted in Fig. 8. A10 biaxial extension produced the starkest contrast between very high and very low  $\sigma_{\min}$  respectively inside and outside the gauge area. Low stresses are instead more evenly spread over the whole surface for A00 and A05.

Finally, for the sake of validation and comparison, full field and load cells data were used to infer the material Young modulus, which had independently been measured in a uniaxial tensile test, as described earlier, together with Poisson's ratio. This estimates were carried out in a range of ways representing commonly adopted methods, and all of them included the knowledge of  $\nu = 0.39$  and the assumption of plane stress and isotropic linear elasticity. The graphical representation of these results are depicted in the histogram of Fig. 9.

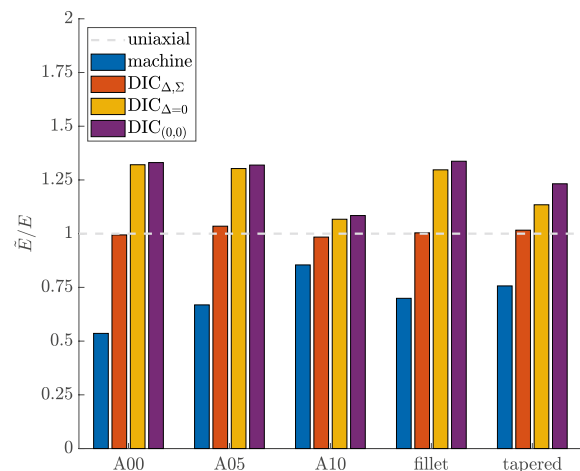
For all samples, the evaluation of equation (11) assisted only by load cells data underestimated the true value of  $E$ , as measured in simple extension (see Fig. 9, blue bars). Understandably, the best so-computed Young modulus estimate corresponded to our A10 sample, since this was the closest to the *blind* assumptions of perfect biaxiality and had the


**Fig. 7** Minimum and maximum gauge area principal stresses. Values normalized by  $E/(1 - \nu^2)\bar{\epsilon}$ 

**Fig. 8** Minimum principal stress from FEM simulations. From left to right: A00, A05, A10. Stress normalized by  $E/(1 - \nu^2)\bar{\epsilon}$ 

highest gauge strain level (see Fig. 6(a)). Its estimate error was about 15%. All other estimates did not pass 75% of  $E$ . Again, the large fillet radii samples represented the worst case, since they exhibited both a low level of equibiaxiality and strain transmission.

The evaluation procedure equation (12), simulating the use of an extensometer or biaxial strain gages in the specimen middle, differently from the machine data only exploitation, overestimated the Young modulus (see Fig. 9, purple bars). This is expected, since  $\bar{\epsilon}/\Sigma(0) > 1$  for all samples, thus the higher  $\Sigma(0)$ , the lower this estimate. Therefore,  $\tilde{E}$  obtained from our sample A10 produced the closest guess with  $\tilde{E}/E = 1.08$ , with the second best guess coming from the tapered profile with  $\tilde{E}/E = 1.23$ .

Only the application of equation (13), for all considered specimens, allowed matching exactly the Young modulus obtained from uniaxial extension within experimental uncertainty (see Fig. 9, red bars). Evidently, this derives from exploiting all the available DIC information about the gauge line strain field and validates the DIC readings and the linear elastic mechanical model.


**Fig. 9** Parameter identification. Load cells macrostress and DIC strain measurements along the gauge line are used to infer the Young modulus already known from the uniaxial test in four different ways

As a comparison, in Fig. 9, yellow bars, an estimate which neglects tangential strains ( $DIC_{\Delta=0}$ ) can be computed. In fact, by assuming perfect biaxiality within the gauge area,  $\Delta = 0$  can be substituted in equation (13). This method returns  $\tilde{E}$  similar to equation (12), since  $\Sigma$  is pretty constant along the gauge line ( $\Sigma(0) \approx \langle \Sigma \rangle$ ), except that for the tapered specimen. The difference between this latter estimate and that of the full equation (13) shows the non negligible contribution of the unwanted tangential strain  $\Delta$  to the elastic problem.

## Discussion

Biaxial tests are extremely useful for the investigating materials mechanical behavior. However, achieving accurate experimental measurements can be challenging due to the discrepancy between the desired deformation state and the inevitably inhomogeneous state achievable in testing. A range of approaches are usually adopted for overcoming these difficulties. However, the material science community is still in discussion regarding standard testing procedures, encompassing both measurement techniques and specimen shapes.

With this work, we enrich this discussion from different points of view: performance objectives measures; newly proposed cruciform shapes; simplification of parameters identification.

Other authors have already noticed that both biaxiality and strain transmission losses must be minimized in order to obtain easy-to-handle data and high strain levels in the gauge area. Remedies for reducing one of these two losses have been repeatedly proposed, but the derived engineering solutions do not simultaneously eliminate all the shortcomings. The present multi-objective cost function includes both losses. Accordingly, it establishes two metrics along a line rather than either in specific points or over all the sample surface. This quantification leads to simply but accurately interpret relations between stresses and measured forces, as it is demonstrated in Fig. 9. This is crucial, since an obstacle toward wide adoption of biaxial tests is represented by the difficulty of mapping stresses to measured forces.

The FEM simulations used for the specimen design, even though carried out by means of simplified constitutive assumptions, have allowed for a quantitative insight into the interplay between shape and behavior thanks to a flexible profile geometric parametrization. In particular, material compressibility, strain transmission and biaxiality optima lead all to different design solutions. The effect of Poisson's ratio, as expected, is to inevitably worsen the performance, based on numerical analysis. On the other hand, optimal shapes obtained with different Poisson's ratios do not differ dramatically (see Fig. 4). This is a relief, since it is not desirable to adopt shapes that depend sensitively

on the same material parameters subject to identification, whereas an overarching experimental goal should be the adoption of standard samples for the same material class. Incidentally, this evidence goes hand in hand with that highlighted by [34] that elastic and elastoplastic specimens can be made in a similar way and still allow for correct parameter identification.

Speaking of shapes, high strain levels were achieved in our FEM based optimization by small fillet radii and large arms with a relatively small gauge area, i.e. with samples resembling tapered profiles or the one used in [35, 36], where the optimization was although qualitative. This is reasonable, since such shapes make the arms stiffer in comparison with the gauge area. Biaxiality, instead, could in theory be improved by large fillet radii, according to our computations. Nevertheless, this improvement has failed to realize in experimental tests. ROI stress quantification confirmed extremely low minimum stresses associated to large fillet radii, which might suggest that, compression has induced local buckling. A further insight into this issue, i.e. the mismatch in predicted versus experimental biaxiality performance, can be retrieved by FEM simulations. A00 and A05 presented low stresses over the hole domain, while A10 only over the arms. This could suggest that A10 performed well also in terms of biaxiality because hoop instability in the arms is a similar mechanism to the insertion of hooks or slots in lowering the gauge area tangential strains: it decouples tangential and normal stresses. This issue, whose detailed evaluation is out of scope here, raises an alarm in terms of experimental interpretation, since local instability can hardly be detected by force measurements or top view image processing. On the other hand, it also indicates one more reason for preferring small fillet radii and small gauge areas which have globally performed better within our metrics. In this case, indeed, all the gauge area is well conditioned in terms of tensile stresses.

Briefly, the presented experimental evidence, has shown that maximizing strain levels in the gauge area in the design process provides samples with a behavior closer to the ideal one than with shapes obtained with the goal of minimizing biaxiality losses. Besides, the effectiveness of small radii has resulted superior to the introduction of profile singularities, in the form of sharp crossroad corners, as it is demonstrated by the better behavior of the newly proposed A10 design in comparison with tapered ones.

The other novel point of this article regards the material characterization procedure, which enables and additional equilibrium equation relating gauge line normal stresses, which are functions of unknown material properties, to load cells measurements (see flowchart Fig. 2). The gauge line is selected in such a way that it lies along a principal direction, so that no tangential stresses need to be accounted for in the equilibrium equation equation (8).

It is noteworthy that the proposed characterization: simplifies the full field measurements since it needs only local information about the deformation process; mitigates the numerical and coding modelling effort in that original constitutive models do not need to be included in finite element computations for simulating the mechanical response of the whole two-dimensional domain.

In this initial application of equilibrium-based material characterization, we focused on the relatively straightforward linear elastic scenario to demonstrate the feasibility of the concept. In linear elasticity is indeed unnecessary to perform both uni- and biaxial test for obtaining the material properties. On the other hand, knowing the linear elastic properties from the uniaxial test has been useful for validation purposes and showed the robustness of the approach.

## Conclusions

The present design procedure relies upon standard deviations from ideal objectives along gauge lines. This facilitates a direct mapping of average stresses to load cell forces. This approach has allowed for the design of shapes that outperform existing ones, at least among simply connected surfaces, which are straightforward to manufacture in common facilities without altering the tested materials. It has not been possible to realize a uniformly equibiaxially stretched gauge area, despite a considerable number of geometry degrees of freedom. The objective of reading load cell data only for inferring mechanical parameters has not been reached entirely, but at best only approached by one new shape. Exclusively the use of full DIC information along the gauge line has allowed to retrieve correctly the material parameters independently measured for all samples. This surely underlines the necessity of improving the reliability and flexibility of DIC procedures in the realm of mechanical characterization [37].

Given the persisting challenges in attaining a sufficiently large purely equibiaxial area, sole reliance on load cell data introduces significant errors, evident even in the linear elastic case. The remaining concern now revolves around achieving optimal strain transmission to explore as large as possible material deformations. In this context, the A10 sample emerges as the most suitable design, surpassing the performance of the tapered alternative.

In this work, we have exploited the fact that our gauge line lies entirely along a principal direction. This allows for testing constitutive equations which are mostly expressed in terms of strain invariants. Of course, in future studies, thinking of anisotropy or general biaxial extension, this line might not be straight and should be individuated by analyzing displacement streamlines.

These considerations help towards extensive investigations into large deformations testing and inelastic,

anisotropic media, which are important frontiers, especially for soft materials, to be pushed for enlarging our knowledge of material mechanics. Even though in this study only small strains have been considered, it is encouraging that, when loading history and inelastic deformations were considered, no dramatic differences were found in optimal shapes or stress levels [6, 34].

**Acknowledgements** G. Vitucci is supported by the POR Puglia FESR-FSE project REFIN A1004.22. The author is extremely grateful to Domenico De Tommasi, Giuseppe Puglisi and Giuseppe Saccomandi for the fruitful discussions which led to this research.

**Funding** Open access funding provided by Politecnico di Bari within the CRUI-CARE Agreement.

## Declarations

**Conflicts of Interest** The author declares not to have competing interests related to the subject matter discussed in this article.

**Open Access** This article is licensed under a Creative Commons Attribution 4.0 International License, which permits use, sharing, adaptation, distribution and reproduction in any medium or format, as long as you give appropriate credit to the original author(s) and the source, provide a link to the Creative Commons licence, and indicate if changes were made. The images or other third party material in this article are included in the article's Creative Commons licence, unless indicated otherwise in a credit line to the material. If material is not included in the article's Creative Commons licence and your intended use is not permitted by statutory regulation or exceeds the permitted use, you will need to obtain permission directly from the copyright holder. To view a copy of this licence, visit <http://creativecommons.org/licenses/by/4.0/>.

## References

- Linka K, Kuhl E (2023) A new family of Constitutive Artificial Neural Networks towards automated model discovery. *Comput Methods Appl Mech Eng* 403:115731
- Blatz PJ, Ko WL (1962) Application of finite elastic theory to the deformation of rubbery materials. *Trans Soc Rheol* 6(1):223–251
- Tiernan P, Hannon A (2014) Design optimisation of biaxial tensile test specimen using finite element analysis. *Int J Mater Form* 7(1):117–123. <https://doi.org/10.1007/s12289-012-1105-8>
- Demmerle S, Boehler JP (1993) Optimal design of biaxial tensile cruciform specimens. *J Mech Phys Solids* 41(1):143–181. [https://doi.org/10.1016/0022-5096\(93\)90067-P](https://doi.org/10.1016/0022-5096(93)90067-P)
- Hannon A, Tiernan P (2008) A review of planar biaxial tensile test systems for sheet metal. *J Mater Process Technol* 198(1–3):1–13
- Avanzini A, Battini D (2016) Integrated experimental and numerical comparison of different approaches for planar biaxial testing of a hyperelastic material. *Advances in Mater Sci Eng* 2016
- Simón-Allué R, Cordero A, Peña E (2014) Unraveling the effect of boundary conditions and strain monitoring on estimation of the constitutive parameters of elastic membranes by biaxial tests. *Mech Res Commun* 57:82–89. <https://doi.org/10.1016/j.mechrescom.2014.01.009>
- Kawabata S, Matsuda M, Tei K, Kawai H (1981) Experimental survey of the strain energy density function of isoprene rubber vulcanizate. *Macromolecules* 14(1):154–162

9. Nolan DR, McGarry JP (2016) On the correct interpretation of measured force and calculation of material stress in biaxial tests. *J Mech Behav Biomed Mater* 53:187–199. <https://doi.org/10.1016/j.jmbbm.2015.08.019>
10. Zhao X, Berwick ZC, Krieger JF, Chen H, Chambers S, Kassab GS (2014) Novel design of cruciform specimens for planar biaxial testing of soft materials. *Exp Mech* 54(3):343–356. <https://doi.org/10.1007/s11340-013-9808-4>
11. Schemmann M, Lang J, Helfrich A, Seelig T, Böhlke T (2018) Cruciform specimen design for biaxial tensile testing of SMC. *J Compos Sci* 2(1):12. <https://doi.org/10.3390/jcs2010012>
12. Imtiaz H, Fang Y, Du J, Liu B (2019) Fundamental problem in optimizing the biaxial testing specimen. *Sci China Technol Sci* 62(5):773–780. <https://doi.org/10.1007/s11431-018-9459-7>
13. Dexl F, Hauffe A, Markmiller J, Wolf K (2023) Numerical optimization-based design studies on biaxial tensile tests. In: *Proceedings of the Institution of Mechanical Engineers, Part C: Journal of Mechanical Engineering Science* p 095440622311527. <https://doi.org/10.1177/09544062231152773>
14. Chen J, Zhang J, Zhao H (2022) Designing a cruciform specimen via topology and shape optimisations under equal biaxial tension using elastic simulations. *Materials* 15(14):5001
15. Lamkanfi E, VanPaepegem W, Degrieck J, Ramault C, Makris A, VanHemelrijck D (2010) Strain distribution in cruciform specimens subjected to biaxial loading conditions. Part 2: Influence of geometrical discontinuities. *Polym Test* 29(1):132–138
16. Abdelhay AM, Dawood OM, Bassuni A, Elhalawany EA, Mustafa MA (2009) A Newly Developed Cruciform Specimens Geometry for Biaxial Stress Evaluation Using NDE. 13th international conference on Aerospace Sciences and Aviation Technology, ASAT-13-2009-9p
17. Zhu Z, Lu Z, Zhang P, Fu W, Zhou C, He X (2019) Optimal design of a miniaturized cruciform specimen for biaxial testing of TA2 alloys. *Metals* 9(8):823. <https://doi.org/10.3390/met9080823>
18. Makris A, Vandenbergh T, Ramault C, Van Hemelrijck D, Lamkanfi E, Van Paepegem W (2010) Shape optimisation of a biaxially loaded cruciform specimen. *Polym Test* 29(2):216–223. <https://doi.org/10.1016/j.polymertesting.2009.11.004>
19. Seibert H, Scheffer T, Diebels S (2014) Biaxial testing of elastomers - experimental setup, measurement and experimental optimisation of specimen's shape. *Technische Mechanik* 34(2):72–89; ISSN 2199-9244. p 2, 26 MB. Artwork Size: 2,26 MB Medium: application/pdf Publisher: Otto von Guericke University Library, Magdeburg, Germany. <https://doi.org/10.24352/UB.OVGU-2017-054>
20. Bauer J, Priesnitz K, Schemmann M, Brylka B, Böhlke T (2016) Parametric shape optimization of biaxial tensile specimen: Parametric shape optimization of biaxial tensile specimen. *PAMM* 16(1):159–160. <https://doi.org/10.1002/pamm.201610068>
21. Yang X, Wu ZR, Yang YR, Pan Y, Wang SQ, Lei H (2023) Optimization design of cruciform specimens for biaxial testing based on genetic algorithm. *J Mater Eng Perform* 32(5):2330–2343. <https://doi.org/10.1007/s11665-022-07258-6>
22. Gower MRL, Shaw RM (2010) Towards a Planar Cruciform Specimen for Biaxial Characterisation of Polymer Matrix Composites. *Appl Mech Mater* 24–25:115–120. <https://doi.org/10.4028/www.scientific.net/AMM.24-25.115>
23. Ramault C, Makris A, Van Hemelrijck D, Lamkanfi E, Van Paepegem W (2011) Comparison of different techniques for strain monitoring of a biaxially loaded cruciform specimen: strain monitoring of a biaxial test. *Strain* 47:210–217. <https://doi.org/10.1111/j.1475-1305.2010.00760.x>
24. Hartmann S, Gilbert RR, Sguazzo C (2018) Basic studies in biaxial tensile tests: Biaxial tensile experiments. *GAMM-Mitteilungen* 41(1):e201800004. <https://doi.org/10.1002/gamm.201800004>
25. Lamkanfi E, Van Paepegem W, Degrieck J (2015) Shape optimization of a cruciform geometry for biaxial testing of polymers. *Polym Test* 41:7–16. <https://doi.org/10.1016/j.polymertesting.2014.09.016>
26. Cottrell JA, Hughes TJ, Bazilevs Y (2009) *Isogeometric analysis: toward integration of CAD and FEA*. John Wiley & Sons
27. Geuzaine C, Remacle JF (2009) Gmsh: A 3-D finite element mesh generator with built-in pre- and post-processing facilities. *Int J Numer Meth Eng* 79(11):1309–1331
28. Malinen M, Raaback P (2013) Elmer finite element solver for multiphysics and multiscale problems. *Multiscale Model Methods Appl Mater Sci* 19:101–113
29. Wintzer A, Schröder M, Kunwar A, Chapra M, Bates D, Gillam T (2023) *nemocrys/pyelmer: pyelmer v1.1.5*. Zenodo. Available from: <https://doi.org/10.5281/zenodo.7655903>
30. Virtanen P, Gommers R, Oliphant TE, Haberland M, Reddy T, Cournapeau D et al (2020) *SciPy 1.0: fundamental algorithms for scientific computing in Python*. *Nat Methods* 17(3):261–272
31. Thakolkaran P, Joshi A, Zheng Y, Flaschel M, De Lorenzis L, Kumar S (2022) NN-EUCLID: Deep-learning hyperelasticity without stress data. *J Mech Phys Solids* 169:105076
32. Vitucci G, De Tommasi D, Puglisi G, Trentadue F (2023) A predictive microstructure inspired approach for anisotropic damage, residual stretches and hysteresis in biodegradable sutures. *Int J Solids Struct* 270:112232
33. Blaber J, Adair B, Antoniou A (2015) Ncorr: open-source 2D digital image correlation matlab software. *Exp Mech* 55(6):1105–1122
34. Bertin MBR, Hild F, Roux S (2016) Optimization of a Cruciform Specimen Geometry for the Identification of Constitutive Parameters Based Upon Full-Field Measurements: Optimization of a Cruciform Specimen Geometry. *Strain* 52(4):307–323. <https://doi.org/10.1111/str.12178>
35. Bell B, Nauman E, Voytik-Harbin S (2012) Multiscale strain analysis of tissue equivalents using a custom-designed biaxial testing device. *Biophys J* 102(6):1303–1312
36. Putra KB, Tian X, Plott J, Shih A (2020) Biaxial test and hyperelastic material models of silicone elastomer fabricated by extrusion-based additive manufacturing for wearable biomedical devices. *J Mech Behav Biomed Mater* 107:103733
37. Reu PL, Blaysat B, Andò E, Bhattacharya K, Couture C, Couty V et al (2022) DIC Challenge 2.0: developing images and guidelines for evaluating accuracy and resolution of 2d analyses: focus on the metrological efficiency indicator. *Exp Mech* 62(4):639–654

**Publisher's Note** Springer Nature remains neutral with regard to jurisdictional claims in published maps and institutional affiliations.